Proc. Natl. Acad. Sci. USA
Vol. 93, pp. 5747–5752, June 1996
Biophysics

Miniature endplate current rise times <100 μs from improved dual recordings can be modeled with passive acetylcholine diffusion from a synaptic vesicle

(voltage clamp/extracellular recording/Monte Carlo simulation/fusion pore)

JOEL R. STILES*, DIRK VAN HELDEN†, THOMAS M. BARTOL, JR.‡, EDWIN E. SALPETER§, AND MIRIAM M. SALPETER*¶

*Section of Neurobiology & Behavior, Cornell University, Ithaca, NY 14853; †Discipline of Human Physiology, Faculty of Medicine and Health Sciences, The University of Newcastle, Callaghan, NSW 2308, Australia; ‡Computational Neurobiology Laboratory, The Salk Institute, La Jolla, CA 92037; and §Departments of Physics and Astronomy, Cornell University, Ithaca, NY 14853

Contributed by Edwin E. Salpeter, February 7, 1996

ABSTRACT **We recorded miniature endplate currents (mEPCs) using simultaneous voltage clamp and extracellular methods, allowing correction for time course measurement errors. We obtained a 20–80% rise time (t_r) of ≈80 μs at 22°C, shorter than any previously reported values, and t_r variability (SD) with an upper limit of 25–30 μs. Extracellular electrode pressure can increase t_r and its variability by 2- to 3-fold. Using Monte Carlo simulations, we modeled passive acetylcholine diffusion through a vesicle fusion pore expanding radially at 25 nm·ms^{-1} (rapid, from endplate Ω figure appearance) or 0.275 nm·ms^{-1} (slow, from mast cell exocytosis). Simulated mEPCs obtained with rapid expansion reproduced t_r and the overall shape of our experimental mEPCs, and were similar to simulated mEPCs obtained with instant acetylcholine release. We conclude that passive transmitter diffusion, coupled with rapid expansion of the fusion pore, is sufficient to explain the time course of experimentally measured synaptic currents with t_rs of less than 100 μs.**

Neurotransmitter release is a form of exocytosis, a general process of vesicle fusion and pore formation, allowing release of vesicle contents. The small size of transmitter vesicles has prevented direct measurement of pore formation and expansion at synapses, but these processes have been studied extensively for large endocrine vesicles, such as mast cell granules (1–3). These studies have raised interesting questions about whether the pore opening rate and emptying mechanisms underlying mast cell exocytosis would suffice for fast synaptic currents.

Khanin and coworkers (4) used analytic methods to model passive diffusion of acetylcholine (ACh) through a cylindrical fusion pore. They assumed that the pore expanded at the slow rate seen in mast cells (<1 nm·ms^{-1}, 23°C; ref. 2) and predicted that the appearance of ACh in the synaptic cleft would be too slow for miniature endplate current (mEPC) generation. They considered more rapid pore expansion unlikely and concluded that passive diffusion cannot account for ACh release.

However, synaptic Ω figure (fused open vesicle) appearance suggests that pore opening for ACh vesicles is 1–2 orders of magnitude faster than that for mast cell granules. Using rapid freezing of frog endplates after nerve stimulation, Torri-Tarelli and coworkers (5) found that Ω figures appeared during a single 500-μs interval after the synaptic delay. From this and the pore's typical size (radius up to ≈12 nm), the radial expansion rate must be at least 25 nm·ms^{-1} (20°C). Furthermore, the Ω figures did not appear to close, swell, or collapse during a length of time much longer than the duration of mEPCs. These findings led us to ask whether passive ACh diffusion through a pore expanding at 25 nm·ms^{-1} could generate mEPCs comparable with those seen experimentally.

Resolution of this issue depends on accurate measurement of the mEPC rising phase. The rise time can be estimated using an extracellular (EC) microelectrode (e.g., ref. 6) or voltage clamp (VC; e.g., refs. 7 and 8), but technical artifacts can plague both methods, and present literature values vary by up to 4-fold (9). We used VC together with EC recording to identify and correct for measurement errors and obtained a 20–80% rise time (t_r) of only ≈80 μs (22°C).

To model ACh release and mEPC generation, we wrote a program (to be called MCELL) based on our earlier Monte Carlo algorithms (10, 11). Simulated mEPCs obtained with rapid pore expansion closely reproduced both our experimental mEPCs and simulation results obtained with instant ACh release. We conclude that passive diffusion coupled with rapid pore opening is indeed sufficient for efficient generation of fast synaptic currents, and we discuss possible mechanisms that could underlie rapid opening of synaptic vesicles.

MATERIALS AND METHODS

mEPC Recordings. Lizard (*Anolis carolinensis*) ribcages were dissected to expose single layers of muscle fibers. The bathing medium was a reptile Ringer's solution (8). Individual endplates were visualized directly using Hoffman modulation optics. Temperature was held at 22°C.

For VC, we built an amplifier and low capacitance headstages based on earlier designs (8). Microelectrode resistances were only 1–2 MΩ (3 M KCl) after beveling in a silicon carbide slurry. Good penetrations were identified by stable resting potentials of −80 to −90 mV. Such conditions were essential for low noise, wide bandwidth (−3 db at ≈15 kHz while immersed), and fast clamp speed (20–80% time for change in holding potential, V_h). We built a model muscle cell circuit (400 kΩ in parallel with 5 nF) and injected known test currents (analog mEPCs generated electronically) into it across a 40-MΩ resistance (ion channel conductance). The model cell was then clamped to record the analog mEPCs, and accuracy was optimized by adjusting the time constant of the series resistive-capacitive (RC) network used to measure clamp current (12). Analog mEPCs were also used to select a low pass filter cutoff of 9 kHz (−3 db; Kron-Heit,

The publication costs of this article were defrayed in part by page charge payment. This article must therefore be hereby marked "*advertisement*" in accordance with 18 U.S.C. §1734 solely to indicate this fact.

Abbreviations: ACh, acetylcholine; mEPC, miniature endplate current; t_r, 20–80% rise time; EC, extracellular; VC, voltage clamp; V_h, ΔC_p holding potential; RC, resistive-capacitive; L_d, random walk mean step length; D, diffusion constant; h, vesicular fusion pore height; r, pore radius; D_{ACh}, D for ACh in free solution; D_p, D for ACh inside pore; ΔC_p, the concentration across the pore; C_v, the average vesicular concentration.

¶To whom reprint requests should be addressed.

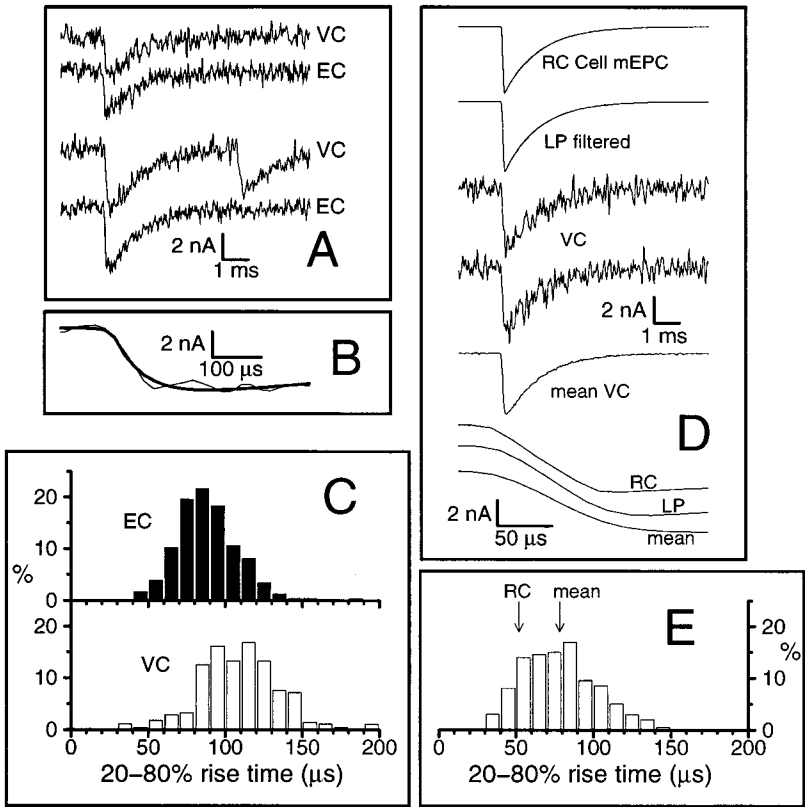

FIG. 1. mEPC t_r. (*A*) Typical VC and EC traces obtained with simultaneous recording and light EC pressure. Lower pair includes mEPC originating from an endplate region not covered by the EC tip. EC traces (measured as voltage) are scaled to match VC amplitude (current). $V_h = -85$ mV; clamp speed = ≈20 μs. (*B*) Fitting mEPCs. The lowest trace from *A* (thin line, expanded scale) is shown with the curve (thick line) obtained from least squares fitting. (*C*) Frequency distributions for t_r. (*Upper*) EC recording (one cell, minimal pressure, $n = 236$). (*Lower*) VC (two cells, $n = 279$, $V_h = -70$ or -85 mV, clamp speed = ≈20 μs). (*D*) Determining VC accuracy. (*Upper*) First (top) trace, direct measurement of analog mEPCs injected into model cell (RC) circuit (50 signals averaged, $t_r = 52$ μs, SD = 0.34 μs). Second trace, after low pass (LP) filtering used for all VC data (50 signals, $t_r = 56$ μs, SD = 0.58 μs). Third and fourth traces, VC traces for the analog mEPC (clamp speed = 20 μs). Fifth trace, average of 200 VC traces ($t_r = 78$ μs). (*Lower*) RC, LP, and mean VC traces on expanded scale. (*E*) Distribution of VC t_r values obtained in *D*. Arrows indicate known t_r (RC) of the analog mEPC and the mean of the VC values.

Avon, MA; model 3750; 4 pole Bessel), which did not prolong t_r significantly. Filtered clamp output was digitized (50 kHz) using a 16-bit stereo audio/digital-signal-processor port interface (Ariel Proport, Highland Park, NJ; model 656), and time epochs (20 ms) containing individual mEPCs were identified and stored on a SUN Sparcstation IPC. Off-line analysis included subtraction of minor baseline drift followed by nonlinear least squares fitting to determine t_r. A subplex fitting algorithm was used with an analytic formula comprising exponential rising and falling phases, as well as a higher order term to fit the shape of the peak. After fitting, mEPC traces could be aligned by their half-amplitude times for signal averaging. Holding potentials were between -50 and -100 mV, and we verified that t_r shows little dependence on V_h (e.g., ref. 7).

For EC recordings, blunt microelectrodes with diameters of 10–30 μm were filled with Ringer's solution (0.25–1.0 MΩ, −3 db at >10 kHz while immersed). An ac amplifier (A-M Systems, Everett, WA; model 1700) was used with low pass filtering at 10 or 20 kHz (−3 db, 2 pole Butterworth). Digitization and off-line fitting were done as for VC records.

For simultaneous recording, the VC electrodes were inserted directly under the visualized endplate, and VC recording was begun. The EC electrode tip was then slowly moved down over the endplate until detectable EC signals could also be seen (defined as minimal pressure; little or no dimpling of endplate membrane). Several hundred events were recorded simultaneously within ≈5 min. The EC electrode was then pushed harder onto the endplate (increased pressure; distinct dimpling), and more events were recorded simultaneously. The actual EC pressure was not quantified and would depend on many factors, including tip size and the mechanical stability of the muscle fiber. With favorable VC penetrations, the cell could be held long enough to continue increasing or decreasing the EC pressure in several stages.

Computer Modeling. MCELL serves as a general Monte Carlo simulator of ligand diffusion and chemical signaling in physiological systems. The mean ± *x*, *y*, and *z* step length (L_d) for diffusing molecules per timestep (Δt) is $\sqrt{(4D\Delta t/\pi)}$, where D is the diffusion constant. Binding and other molecular reaction steps are handled by comparing the event's probability with a random number (10).

Similar to previous studies (10, 13), we modeled the lizard endplate using ≈30 μm² of axonal membrane and ≈170 μm² of folded muscle membrane. To simulate ACh release at an active zone, we added a presynaptic vesicle located above a junctional fold. The vesicle was connected to the axonal membrane through a cylindrical pore that opened instantaneously to an initial height h and radius r. These dimensions could either remain constant or change incrementally. The vesicle was cube-shaped for convenience (see *Results*), with a volume of 2.7×10^4 nm³ (14). ACh receptor binding sites were present at the tops of folds and at decreasing density within the folds (15). The density of acetylcholinesterase binding sites was uniform throughout all cleft spaces (16). The reaction mechanisms and site densities were as given (13). Simulations were run at the Cornell Theory Center, Ithaca, NY, on an IBM ES9000, SP2, or RS6000. (Fig. 5 was rendered using IBM DATAEXPLORER software.)

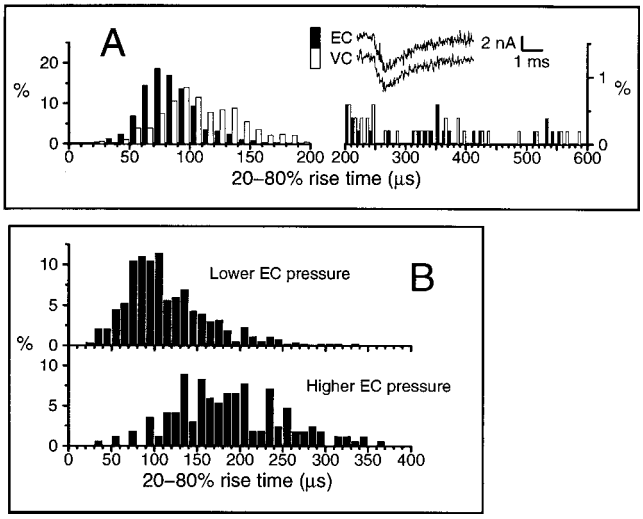

FIG. 2. EC pressure effects. (*A*) Simultaneous recording, high pressure ($n = 512$, $V_h = -50$ mV, clamp speed = ≈20 μs). EC mean = 99 μs; SD = 73 μs. VC mean = 123 μs; SD = 72 μs. VC values are offset as expected (cf. Fig. 1*C*). Both distributions include prolonged t_rs (e.g., inset traces with t_r = ≈200 μs) that were not present when pressure was light or absent. (*B*) EC recording. Pressure can shift and widen the entire t_r distribution. Electrode tip size was <5 μm, rather than the typical 10–30 μm. (*Upper*) Low pressure. Mode = ≈90 μs; mean = 114 μs; SD = 49 μs; $n = 536$. (*Lower*) Same cell, increased pressure. Mean = 192 μs; SD = 74 μs; $n = 169$.

RESULTS

mEPC Recordings. EC recording of the mEPC time course requires only simple electronics, but the EC pressure can lead to occasional prolonged events (6). This raises the possibility of systematic t_r overestimation. Pressure artifacts are not a concern with VC, but accurate measurements are complicated by the interaction of finite clamp speed, which increases the apparent t_r, and under- or overdamped stray capacitances, which can alter t_r and the current's shape (17). With either EC or VC recordings, t_r also can be increased by microelectrode or other low pass filtering. We first optimized recording bandwidth and VC circuitry using analog mEPCs injected into a model cell. Thus, the factors of primary concern were pressure artifacts and the limited maximum clamp speed (≈20 μs), which could be attained with endplates.

Fig. 1*A* shows examples of simultaneous recordings for minimal EC pressure. The two traces corresponding to a single mEPC were essentially indistinguishable by eye. Fig. 1*B* illustrates how we fitted traces to obtain t_r.

Fig. 1*C* shows t_r frequency distributions obtained with EC recording alone (minimal pressure; *Upper*) or VC alone (*Lower*). Both distributions are approximately Gaussian. With EC traces, the mode was ≈80 μs, with a mean of 89 μs (SD = 21 μs). With VC, the mean was 109 μs (SD = 26 μs). Thus, the VC distribution was shifted toward longer values by 20–30 μs.

Fig. 1*D* illustrates the use of analog mEPCs and the model cell to determine that recording bandwidth was adequate even for such fast signals, and that the 20- to 30-μs offset between EC and VC t_r distributions was expected from limited clamp speed. Since the fastest signals are most sensitive to filtering, we generated analog mEPCs with a short, essentially constant t_r of 52 μs (Fig. 1*D*, RC traces), i.e., a value from the lower end of the experimental distribution in Fig. 1*C*, *Upper*. Subsequent 9-kHz low pass filtering as used for VC increased this value by only 4 μs (Fig. 1*D*, LP traces). Overall filtering for EC recording was even milder than for VC (see *Materials and Methods*), so none of our data reflected appreciable t_r prolongation from filtering. To demonstrate the influence of limited clamp speed, we clamped the model cell using a speed of 20 μs

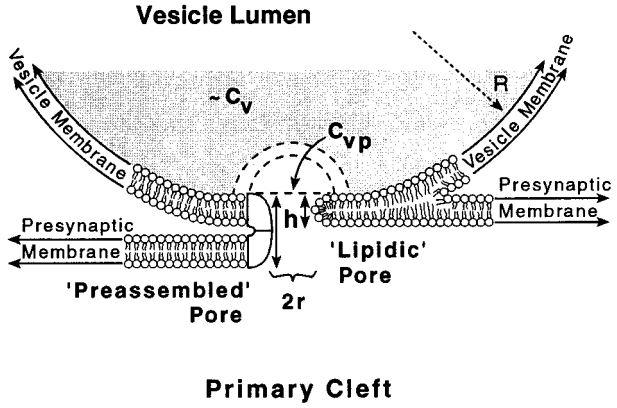

FIG. 3. Fusion pore models. For simulations, h was 9 nm, i.e., between single (right, 6–7 nm) and double (left, 10–12 nm) membrane thickness. C_v, average ACh concentration. The actual concentration decreases close to the pore opening, reaching C_{vp} at the interface between vesicle lumen and inner pore mouth. With vesicle radius $R \gg r$, the gradient ΔC_v is small far from the pore opening. Thus, the simulated vesicle's bounding shape could be a cube to reduce computation time.

(as for endplates) and estimated the known t_r by fitting the VC current for successive analog mEPCs. After alignment and averaging, we obtained a mean trace with a t_r of 78 μs (Fig. 1*D*, VC traces). The result was identical when individual t_r values were averaged. Thus, VC measurements overestimated the actual t_r by 26 μs, mostly due to limited clamp speed as opposed to filtering. The clamp speed-dependent increase in apparent t_r was similar when the known analog mEPC t_r was ≈80 μs rather than ≈50 μs (data not shown).

Recording noise was similar for experimental mEPCs (EC and VC; Fig. 1*A*) and VC analog mEPCs (Fig. 1*D*). The t_r variability obtained by fitting individual traces was also similar for the experimental (Fig. 1*C*) and VC analog (Fig. 1*E*; SD = 24 μs) mEPCs. The t_r distribution for VC analog mEPCs was caused by noise, since the actual analog mEPC t_r SD was <1 μs (see legend Fig. 1*D*, RC cell and LP traces). Therefore, most of the experimental t_r variability also can be attributed to recording noise.

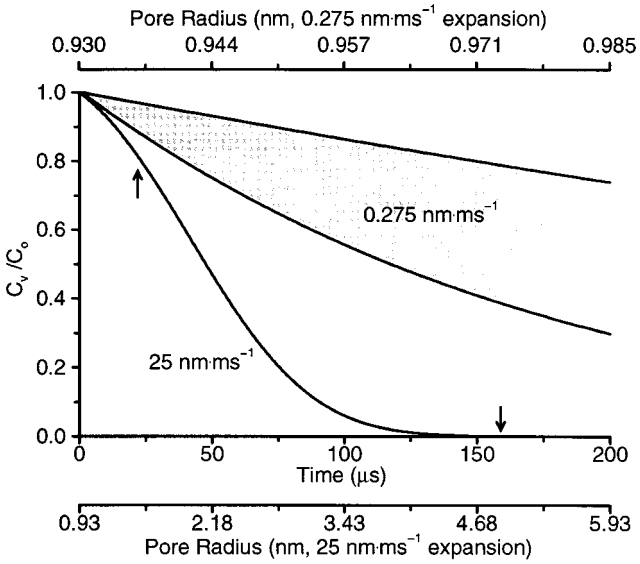

FIG. 4. Vesicle emptying for rapid (25 nm·ms^{-1}) or slow (0.275 nm·ms^{-1}) pore expansion. Simulations started with $r = 0.93$ nm (300 pS). Monte Carlo simulation results were fitted to obtain smooth curves. $D_p = D_{ACh}$ for the bottom and middle curves; $D_p = D_{ACh}/4$ for the top curve. Arrows indicate the times for Fig. 5.

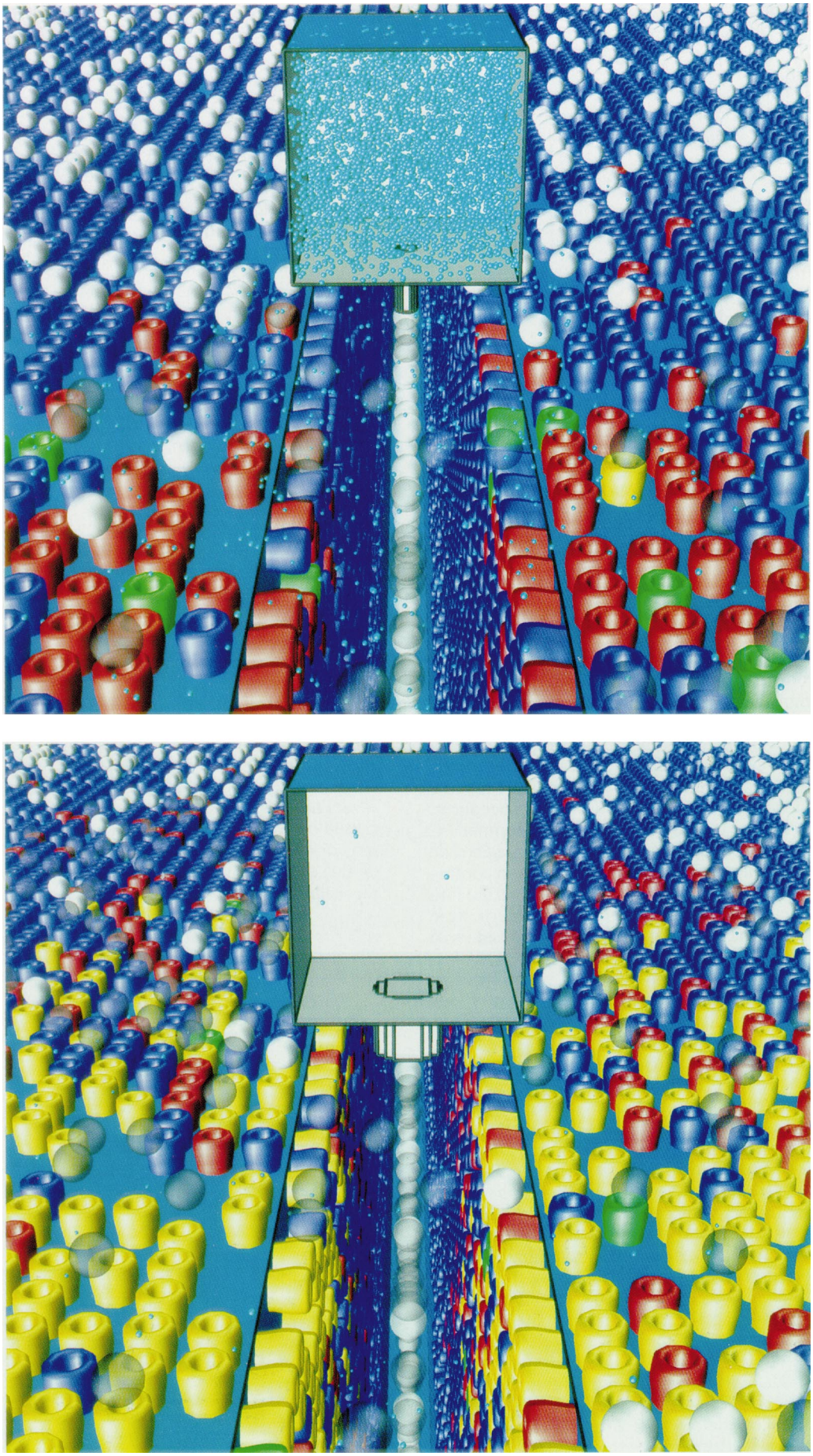

FIG. 5. (*Legend appears on opposite page.*)

Subtracting a 26-μs offset from the mean of 109 μs in Fig. 1*C* (*Lower*) suggests that the actual t_r for endplates is about 83 μs, very close to the mode of $\approx$80 μs in Fig. 1*C* (*Upper*). In five experiments using EC recording and minimal to moderate pressure, we always obtained a t_r mode of 70–90 μs (eight cells, mean = 97 μs, SD = 34 μs, n = 1077). A similar mode was generally seen when EC pressure was high during simultaneous recording, but both EC and VC t_r distributions were strongly skewed toward longer values (130–600 μs; Fig. 2*A*). This pressure-dependent appearance of long t_rs was mostly reversible (three experiments, five cells, n = 1862). In one experiment, however, we used an EC electrode tip smaller than the usual 10–30 μm and found that increased pressure shifted and widened the entire t_r distribution, essentially doubling the apparent mean and tripling the variability (Fig. 2*B*). Regardless of tip size, high pressure also gave rise to occasional mEPCs with t_rs in excess of 1 ms and a prolonged falling phase.

Our electrophysiological findings clearly establish that few if any normal mEPCs have a t_r longer than 100–110 μs in this preparation and that the rising phase shape can be measured most accurately from those EC traces that constitute the mode of distributions like those shown in Figs. 1*C* (*Upper*) and 2*A*. Accordingly, we aligned and averaged such events (individual apparent t_rs between 70 and 90 μs) to obtain an experimental result that we then used to test our simulations of ACh release and mEPC generation (see Fig. 6*C*).

Computer Simulations. A t_r of only $\approx$80 μs indicates extremely fast ACh release. While many factors might influence ACh movement, we determined whether passive diffusion alone could suffice.

Vesicular release: Theoretical basis and simulation accuracy. Net ACh flux depends on ΔC_p (the concentration gradient across the pore), the pore's area, and D for ACh within the pore (D_p, which may not be the same as in free solution, D_{ACh}; see below). ΔC_p depends primarily on C_v, the average vesicular concentration, but also in part on gradients from the inner pore mouth to the vesicle interior (ΔC_v; Fig. 3). If ΔC_v is ignored, then vesicle emptying can be predicted analytically for fixed pore dimensions (1) or radial pore expansion at a constant rate (4). However, emptying time is thereby underestimated, and the error depends on $\Delta C_v/\Delta C_p$. For rapid expansion, the error becomes appreciable and ΔC_v cannot be ignored.

To simulate ΔC_v and ΔC_p accurately, L_d had to be small compared with r. With constant h and r, vesicle emptying follows an exponential decay and we obtained <4% error with $(L_d/r) \leq 0.2$. For rapid pore opening, we therefore maintained L_d/r between 0.1 and 0.2, using Δt values that increased from $\approx$10 to $\approx$300 ps.

Vesicle emptying and mEPC generation. D_{ACh} is approximately 6×10^{-6} cm^2·s^{-1} for a dissociated ACh salt under physiological conditions (18). D_p will be $\approx$0 until the pore reaches a size comparable with that of ACh itself ($\approx$0.5 nm radius) and then will increase to D_{ACh} if the pore becomes much larger than ACh. Khanin and coworkers estimated that for $r \approx 1$ nm, hindered diffusion would reduce D_p to $\approx D_{ACh}/4$ (4). This would be the case if the pore opened slowly, as for mast cell granules (0.275 nm·ms^{-1}, calculated from Fig. 2D in ref. 2). Even with $D_p = D_{ACh}$, the time for vesicle emptying with such slow expansion would greatly exceed t_r (Fig. 4). With rapid expansion ($\geq$25 nm·ms^{-1}; see Introduction), however, r would greatly exceed ACh's size by the time appreciable emptying began. Then, with $D_p = D_{ACh}$, the time for 80% emptying would be comparable with t_r (Fig. 4), and the vesicle would empty as the pore approached endplate Ω figure dimensions (Figs. 4 and 5).

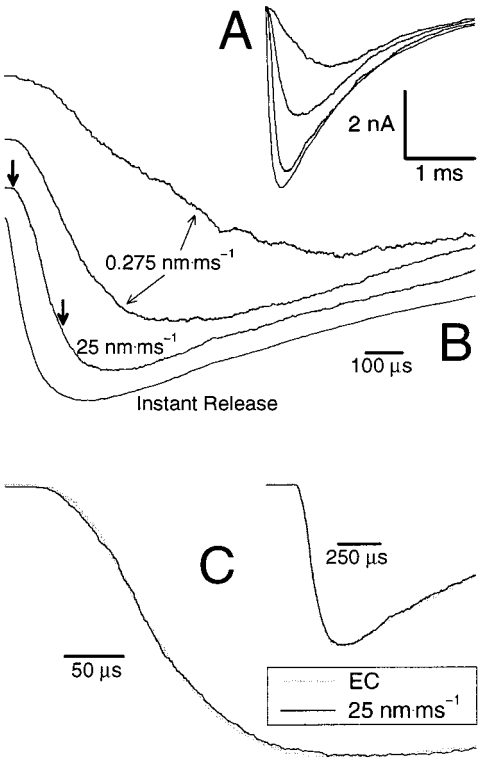

FIG. 6. Simulated and experimental mEPCs. (*A*) Simulated mEPCs obtained with slow or rapid expansion as in Fig. 4 (labeled in *B*), plus limiting case of instant ACh release (lowest trace). (*B*) Same traces on expanded time scale (normalized by amplitude). Heavy arrows indicate the times for Fig. 5. (*C*) Comparison of the experimental mEPC time course (EC modal events averaged from Figs. 1*C* and 2*A*; n = 281) and the simulated mEPC obtained with 25 nm·ms^{-1} pore expansion (same traces shown on two scales).

Fig. 5 shows images from a simulation of ACh release through a rapidly expanding pore, diffusion within the synaptic cleft, activation of postsynaptic ACh receptors, and hydrolysis by acetylcholinesterase. Fig. 6*A* shows four simulated mEPCs, three corresponding to the different pore opening rates and conditions of Fig. 4 and one corresponding to the limiting case where all ACh molecules were released instantly. D for ACh within the synaptic cleft was about 2-fold smaller than D_{ACh}, consistent with impeded movement through basal lamina material (19).

The t_r and amplitude obtained with 25 nm·ms^{-1} expansion were nearly identical to those obtained with instant ACh release (Fig. 6 *A* and *B*). Furthermore, Fig. 6*C* shows that the simulated mEPC was essentially identical to our averaged experimental mEPC, matching not only t_r but also the shape of the rising phase and peak. Simulation of slow expansion (0.275 nm·ms^{-1}) gave a 2- to 5-fold increase in t_r, a broader peak, and a 2- to 3-fold reduction in amplitude (Fig. 6 *A* and *B*). With slow expansion, the experimental t_r, shape, and amplitude could not be reproduced.

FIG. 5. (*Legend from previous page.*) Simulation of ACh release and mEPC generation. The vesicle cube sits above the 50-nm-high primary cleft, over a junctional fold (50 nm wide, 800 nm deep). Axonal membrane and front vesicle wall are transparent. Pore expansion rate was 25 nm·ms^{-1}. Free ACh, blue spheres (0.7-nm diameter). Bound AChs not shown. ACh receptors, unbound = blue, one ACh bound = red, two AChs bound = green (closed channel) or yellow (open channel). Acetylcholinesterase spheres lie within primary cleft and fold spaces; unbound = white, hydrolyzing ACh = translucent gray. (*Upper*) Twenty-two microseconds after pore opens (r = 1.5 nm, vesicle $\approx$80% full, channel opening begins). (*Lower*) One hundred thirty-eight microseconds later (r = 5 nm, vesicle nearly empty, amplitude $\approx$80% of peak).

DISCUSSION

Our t_r value for mEPCs (≈80 μs, SD appreciably less than ≈30 μs) is faster than any previous values and was obtained with EC recording in combination with quantitatively optimized VC. We found that EC pressure can produce occasional slow mEPCs (Fig. 2*A*), as already noted by Katz and Miledi (6), who suggested that the cause is partial occlusion of the primary cleft (impeded ACh diffusion). We also found, however, that EC pressure can markedly increase the apparent mean t_r and its variability (Fig. 2*B*). This may explain many of the long t_r values in the literature (e.g., ref. 9). The fact that pressure-dependent mEPC changes were also reflected in simultaneous VC recordings proves that actual changes in synaptic microphysiology or anatomy are responsible, rather than an EC measurement artifact. Further study would be required to determine the relative importance of possible factors such as cleft occlusion, altered ACh release, or altered channel gating. Our aim was to avoid any changes in the normal t_r and shape.

Using quantitative Monte Carlo simulations, we have shown that the size and fast time course of experimental mEPCs can be matched if vesicular ACh diffuses passively through a fusion pore expanding at a rapid rate (25 $nm \cdot ms^{-1}$) suggested by endplate Ω figure appearance (5). Although mechanisms more complex than passive diffusion could conceivably contribute to ACh release, we have shown that they are not necessary.

How could a fusion pore open at 25 $nm \cdot ms^{-1}$ or even faster? It has been suggested that a purely lipidic pore (see Fig. 3) could form and expand when the highly curved (stressed) vesicle wall and dimpled presynaptic membrane are drawn very close together by active contractile processes (3). This is a reasonable hypothesis, but it remains unclear whether relaxation of lipid bilayer stress could generate enough force to cause sufficiently rapid wall movements in vesicles docked at the active zone, where lipoprotein interactions are present. As a possible alternative, we suggest that pore expansion itself may be actively mediated. The scale of the required movement (5–10 nm radially) is similar to the single step length of certain molecular motors (e.g., kinesin; ref. 20). The very short time required for a single, discrete protein conformational change (i.e., only one step by a molecular motor) would provide the required rapid expansion. Several "cocked springs" could exist in a radial array around the docked vesicle, perhaps linked to a preassembled protein core (Fig. 3) spanning both the vesicle membrane and the presynaptic membrane (1). Once triggered by Ca^{2+} influx, the springs could contract, opening the pore rapidly over a limited distance. A second set of springs oriented circumferentially could even purse-string the pore, drawing it closed on a longer timescale and allowing for possible vesicle reuse. Regardless of such still unproven issues, we conclude that passive diffusion of transmitter, coupled with rapid pore expansion inferred for synaptic vesicles, is sufficient for efficient generation of fast synaptic currents.

We thank Irina Kovyazina for excellent technical assistance; Bruce Johnson, Thomas Podleski, Karl Magleby, William Betz, and Rodney Parsons for helpful comments on the manuscript; and Kathie Burdick for secretarial services. This work was supported by National Institutes of Health Grants K08NS01776 (J.R.S.) and NS09315 (M.M.S.).

1. Almers, W. & Tse, F. W. (1990) *Neuron* **4,** 813–818.
2. Spruce, A. E., Breckenridge, L. J., Lee, A. K. & Almers, W. (1990) *Neuron* **4,** 643–654.
3. Monck, J. R. & Fernandez, J. M. (1994) *Neuron* **12,** 707–716.
4. Khanin, R., Parnas, H. & Segel, L. (1994) *Biophys. J.* **67,** 966–972.
5. Torri-Tarelli, F., Grohovaz, F., Fesce, R. & Ceccarelli, B. (1985) *J. Cell Biol.* **101,** 1386–1399.
6. Katz, B. & Miledi, R. (1973) *J. Physiol. (London)* **231,** 549–574.
7. Gage, P. W. & McBurney, R. N. (1975) *J. Physiol. (London)* **244,** 385–407.
8. Land, B. R., Salpeter, E. E. & Salpeter, M. M. (1980) *Proc. Natl. Acad. Sci. USA* **77,** 3736–3740.
9. Van der Kloot, W. (1995) *Biophys. J.* **69,** 148–154.
10. Bartol, T. M., Jr., Land, B. R., Salpeter, E. E. & Salpeter, M. M. (1991) *Biophys. J.* **59,** 1290–1307.
11. Stiles, J. R. (1990) Ph.D. dissertation (Univ. Kansas, Lawrence, KS).
12. Finkel, A. S. (1985) in *Voltage and Patch Clamping with Microelectrodes*, eds. Smith, T. G., Jr., Lecar, H., Redman, S. J. & Gage, P. W. (Williams & Wilkins, Baltimore), pp. 9–24.
13. Anglister, L., Stiles, J. R. & Salpeter, M. M. (1994) *Neuron* **12,** 783–794.
14. Steinbach, J. H. & Stevens, C. F. (1976) in *Frog Neurobiology*, eds. Llinas, R. & Precht, W. (Springer, New York), pp. 33–92.
15. Salpeter, M. M., Smith, C. D. & Matthews-Bellinger, J. A. (1984) *J. Electron Microsc. Tech.* **1,** 63–81.
16. Salpeter, M. M. (1969) *J. Cell Biol.* **42,** 122–134.
17. Finkel, A. S. & Gage, P. W. (1985) in *Voltage and Patch Clamping with Microelectrodes*, eds. Smith, T. G., Jr., Lecar, H., Redman, S. J. & Gage, P. W. (Williams & Wilkins, Baltimore), pp. 47–94.
18. Dionne, V. E. (1976) *Biophys. J.* **16,** 705–717.
19. Land, B. R., Harris, W. V., Salpeter, E. E. & Salpeter, M. M. (1984) *Proc. Natl. Acad. Sci. USA* **81,** 1594–1598.
20. Meyhofer, E. & Howard, J. (1995) *Proc. Natl. Acad. Sci. USA* **92,** 574–578.